Acta Crystallographica Section D
Biological Crystallography
ISSN 0907-4449

Novel multisubstrate inhibitors of mammalian purine nucleoside phosphorylase

Angela V. Toms, Weiru Wang, Yingbo Li, Bruce Ganem and Steven E. Ealick*

Department of Chemistry and Chemical Biology, Cornell University, Ithaca, NY 14853, USA

Correspondence e-mail: see3@cornell.edu

Received 6 July 2005
Accepted 9 August 2005

PDB References: 2ai1, bPNP with guanosine-2′,3′-*O*-ethylidenephosphonate; 2ai2, bPNP with 9-deazainosine-2′,3′-*O*-ethylidenephosphonate; 2ai3, bPNP with guanosine-2′,3′-*O*-methylidenephosphonate.

In an effort to develop potent multisubstrate-analog inhibitors of purine nucleoside phosphorylase (PNP), three nucleoside phosphonates were designed utilizing structural information from the previously reported structures of complexes of bovine PNP with substrates and products. The nucleoside phosphonates contain an acetal linkage at the O2′ and O3′ positions and a two-C-atom spacer between the ribose and phosphate moieties. The linkage enables the compounds to simultaneously occupy the purine-, ribose- and phosphate-binding sites. The chemical syntheses, inhibition profiles and structural characterization of these novel multisubstrate analog inhibitors with bovine PNP are described.

1. Introduction

Purine nucleoside phosphorylase (PNP; EC 2.4.2.1) catalyzes the reversible phosphorolysis of ribonucleosides to ribose 1-phosphate and the free base. Although equilibrium favors nucleoside synthesis, PNP functions biologically in the phosphorolytic direction as part of the purine-salvage pathway. Interest in PNP arises from its key role in purine nucleoside metabolism and from its role in T-cell development. The therapeutic utility of PNP inhibitors is based on the finding that PNP-deficient patients have little or no T-cell function but have near-normal B-cell response (Giblett *et al.*, 1975). This effect is caused by the accumulation of 2′-deoxyguanosine triphosphate (dGTP) in T cells which have high levels of deoxycytidine kinase. The dGTP subsequently acts as a feedback inhibitor of ribonucleotide reductase and results in selective T-cell toxicity (Cohen *et al.*, 1978). This profile suggests that PNP inhibitors might be used to selectively kill T cells in T-cell leukemias and T-cell lymphomas, to suppress the post-organ transplant T-cell response or to treat T-cell-mediated autoimmune diseases (Ealick *et al.*, 1991).

PNP belongs to the nucleoside phosphorylase-I (NP-I) family of enzymes. The NP-1 enzymes share a common α/β-subunit fold and accept a range of both purine and pyrimidine nucleoside substrates. PNP has been isolated and structurally characterized from both eukaryotic and prokaryotic organisms. Two main classes of PNP have been characterized. The trimeric enzymes, found mainly in mammals, are specific for 6-oxopurine nucleosides and have a monomeric molecular weight of about 31 kDa (Bzowska *et al.*, 1995; Ealick *et al.*, 1990; Koellner *et al.*, 1997; Mao *et al.*, 1998). The second class of PNP, found in many prokaryotes, is hexameric with a monomeric molecular weight of about 26 kDa (Cacciapuoti *et al.*, 1994; Hori *et al.*, 1989; Jensen, 1978; Jensen & Nygaard, 1975; Senesi *et al.*, 1976). Differences in the active-site residues result in different substrate specificity for the two classes of PNP, even though the overall fold is the same. In general,

PNPs with a trimeric structure accept only 6-oxopurine nucleosides as substrates, whereas the hexameric PNPs also accept 6-aminopurine nucleosides. The focus of this paper is in designing an inhibitor for the mammalian enzyme.

Effective *in vivo* inhibitors of PNP have been difficult to obtain, presumably owing to the high levels of PNP in humans, particularly in lymphoid tissues and in erythrocytes, which necessitate a very potent binding affinity. One of the first reported inhibitors of PNP was 8-aminoguanine, which showed a K_i of 0.2 μM (Stoeckler, 1984) with human erythrocyte PNP. An important class of PNP inhibitors are multisubstrate-analog inhibitors. These compounds are designed to mimic both substrates of PNP, the purine nucleoside and phosphate, and as such should interact with the purine-, ribose- and phosphate-binding sites in the enzyme. Some of the first multisubstrate-analog inhibitors tested were the metabolites of the antiherpetic agent acyclovir (Tuttle & Krenitsky, 1984). Despite the favorable binding properties of acyclovir diphosphate, its inability to permeate membranes and its metabolic instability limit its potential as a clinically useful drug. Among the known inhibitors of nucleoside phosphorylases, nucleoside phosphonate analogs are noteworthy. Nucleoside phosphonates contain a phosphonic acid group in place of the naturally occurring phosphate groups. They have similar solubility, polarity and size to phosphates, but are stable to phosphatases under normal dephosphorylation conditions. The goal of this research was to design, synthesize and structurally characterize multisubstrate-analog inhibitors of PNP containing a phosphonate group that would bind in the phosphate-binding pocket of the enzyme.

2. Experimental procedures

2.1. Protein purification

Partially purified purine nucleoside phosphorylase from calf spleen was purchased from Sigma Chemical Co. This protein sample was further purified using a reactive dye-matrix column. All steps were performed at 277 K unless otherwise noted. The Sigma protein was dialyzed against 10 mM MES pH 6.0 and 1 mM dithiothreitol (DTT) (loading buffer). The dialyzed sample was then concentrated to a volume of 5 ml and directly loaded onto a 5 ml green-19 dye-matrix column pre-equilibrated in loading buffer. The column was then washed with excessive loading buffer until the eluate had no detectable protein concentration. A two-step wash gradient was performed with loading buffer supplemented with 0.4 and 0.7 M NaCl. The protein was eluted with loading buffer supplemented with 2 M NaCl and 20 mM ATP. The eluted protein was dialyzed against 10 mM Tris pH 7 and 1 mM DTT and concentrated to 8 mg ml^{-1} based on a Bradford assay.

Table 1
Data-collection and processing statistics.

Values for the outer resolution shell (2.07–2.00 Å for compound 1 and 1.76–1.70 Å for compounds 2 and 3) are given in parentheses.

Compound	(1)	(2)	(3)
Space group	$P2_13$	$P2_13$	$P2_13$
Unit-cell parameter (Å)	93.95	93.24	93.99
Resolution (Å)	2.0	1.7	1.7
Unique reflections	18969	29947	30699
Redundancy	8.9 (8.9)	6.7 (5.9)	8.7 (6.0)
Completeness (%)	99.8 (100)	99.8 (100)	99.3 (98.3)
$I/\sigma(I)$	30.5 (9.8)	23.1 (5.3)	42 (5.0)
R_{sym}†	7.5 (33.9)	5.5 (43.9)	4.6 (44.8)

† $R_{sym} = \sum\sum_i |I_i - \langle I\rangle| / \sum\langle I\rangle$, where $\langle I\rangle$ is the mean intensity of N reflections with intensities I_i and common indices h, k and l.

2.2. Crystallization

Inhibitors were cocrystallized with the enzyme. The reservoir solution contained 100 mM Tris buffer pH 7.2–7.6, 10–12% PEG 2000 MME and 100 mM magnesium acetate with 1 mM potassium phosphate. Each drop was set up with 2 µl protein solution plus 2 µl reservoir solution with an additional 5 mM inhibitor. Crystals appeared from clear drops after about 24 h of equilibration against reservoir solution and reached their maximum size over the course of a few weeks.

2.3. Data collection and processing

The X-ray diffraction data were collected at CHESS station F1. The data was recorded with a Quantum 4 mosaic CCD-based X-ray detector. The crystals were flash-frozen directly from the crystallization drop in a gaseous nitrogen stream immediately before data collection. Each data set was collected using a single crystal. The *HKL*2000 suite (Otwinowski & Minor, 1997) of programs was used for scaling and integration of all data sets. The data-collection statistics are shown in Table 1.

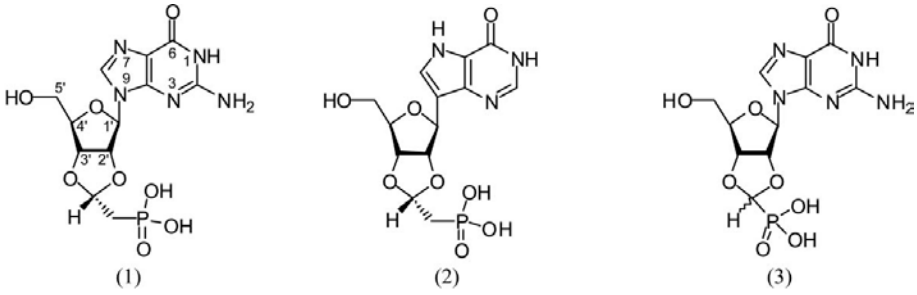

Figure 1
Chemical structures of the multisubstrate-analog phosphonate inhibitors.

2.4. Structure determination

The PNP–inhibitor complex structure determinations and refinements were performed using the *Crystallography & NMR System* (*CNS*; Brünger *et al.*, 1998). The starting model, consisting of the protein atom coordinates from PDB code 1a9p, was first subjected to rigid-body refinement. Simulated-annealing refinement, positional refinement and *B*-factor refine-

ment cycles were then carried out in an iterative manner. σ_A-weighted difference Fourier maps (Read, 1986) were calculated and manual adjustment with the graphics program *O* (Jones *et al.*, 1991) was performed after each refinement cycle. A test set containing 5% of the experimental data was randomly selected and used for free *R* factor calculation. The free *R* factor was used for cross-validation throughout the refinement. The inhibitor topology and parameter files for *CNS* were generated using *PRODRG* (van Aalten *et al.*, 1996). Water molecules were added to the model when the density peaks were at least 2.7σ in an $F_o - F_c$ map and when they formed appropriate hydrogen-bond contacts. The molecular structures of inhibitors were manually fitted into the active site based on the electron density in $F_o - F_c$ and $2F_o - F_c$ maps. They were then refined in the subsequent cycles. The model was examined using *CNS* (Brünger *et al.*, 1998) and *PROCHECK* (Laskowski *et al.*, 1993). The final refinement statistics are summarized in Table 2.

Table 2
Refinement statistics and model building.

Compound	(1)	(2)	(3)
Resolution (Å)	2.0	1.7	1.7
Total No. of non-H atoms	2278	2410	2349
No. of protein atoms	2111	2117	2139
No. of water O atoms	131	258	175
No. of reflections in refinement	17887	27383	28311
No. of reflections in test set	886	1415	1476
R factor† (%)	21.2 (24.3)	19.6 (21.9)	22.1 (25.7)
R_{free}‡ (%)	25.4 (29.4)	23.1 (27.4)	25.3 (28.3)
R.m.s. deviation from ideal geometry			
Bonds (Å)	0.008	0.007	0.008
Angles (°)	1.4	1.5	1.4
Ramachandran plot			
Most favored (%)	90.1	93.9	92.1
Allowed (%)	9.1	5.2	6.6
Generously allowed (%)	0.4	0.4	0.4
Disallowed (%)	0.4	0.4	0.4
Average *B* factors (Å^2)			
Main chain	30.62	24.54	30.22
Side chain	32.37	27.22	32.72
Inhibitor	22.84	26.79	33.6
Solvent	33.29	38.28	37.78

† R factor $= \sum_{hkl} ||F_{obs}| - k|F_{calc}|| / \sum_{hkl} |F_{obs}|$, where F_{obs} and F_{calc} are the observed and calculated structure factors, respectively. ‡ For R_{free}, the sum is extended over a subset of reflections excluded from all stages of refinement: 5% for all data sets.

2.5. Synthesis of PNP inhibitors

Three nucleoside-derived cyclic phosphonoacetals (1)–(3) (Fig. 1) were designed as multisubstrate-analog inhibitors of PNP based on the active-site structure of bovine PNP. Compounds (1) and (2) feature a two-carbon bridge between the ribose ring and the phosphonate group, which was designed to place the phosphate moiety into the phosphate-binding site. The choice of (2) as a target was based on earlier work that showed C-nucleoside analogs incorporating 9-deazahypoxanthine at C1′ formed an extra hydrogen bond between N7 and Asn243 in bovine PNP. Compound (3), having only a single-carbon linker, was synthesized as a control following a published procedure (Endova *et al.*, 1996)

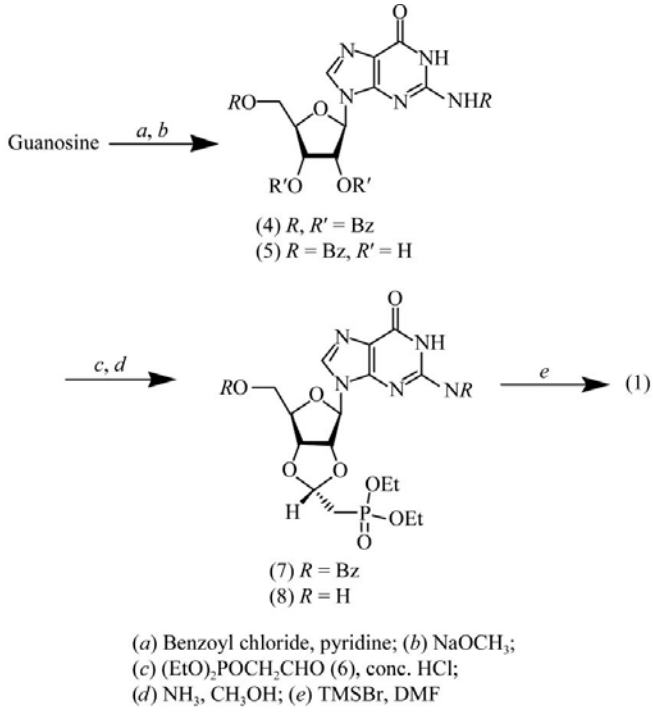

Figure 2
Synthesis of compound (1).

Inhibitor (1) was synthesized in five steps as shown in Fig. 2. Reaction of guanosine with benzoyl chloride produced the known tetrabenzoyl derivative (4) (Chladek & Smrt, 1964), which could be selectively debenzoylated using sodium methoxide (two equivalents) to afford diol (5) in 60% yield. When exposed to phosphonoacetaldehyde (6) or its corresponding diethylacetal in benzene in the presence of various acid catalysts (TsOH, CH_3SO_3H, H_2SO_4), diol (5) failed to form the expected phosphonoacetal (7), returning only unreacted starting material. A literature search revealed an earlier report describing difficulties in forming acetals of guanosine using aliphatic aldehydes (Bakthavachalam *et al.*, 1987). Noting that the diethyl acetal of (6) required heating at reflux with 2.5% HCl to form and concentrated HCl to exchange with other alcohols (Yanai *et al.*, 1980), the use of more concentrated acid catalysts was explored. Indeed, reaction of (5) with a 1:2 weight ratio of aldehyde (6) and concentrated HCl afforded the desired nucleoside acetal (7), which was subjected without extensive purification to debenzoylation (ammonia–methanol) to give acetal (8) in 47% yield, exclusively as its *endo* isomer, which was confirmed by a proton 2D-ROESY experiment. When treated with trimethylsilyl bromide (TMSBr), phosphonodiester (8) was transformed into phosphonate (1) in 54% yield.

Formation of the desired *endo*-acetal (8), albeit in modest yield, as the only isolable product was noteworthy. It is possible that cleavage of the N-glycosidic bond, which was observed under the strongly acidic reaction conditions, may have selectively decomposed the corresponding *exo*-acetal. Nevertheless, a similar *endo*-preference has been noted for acetals of adenosine with aliphatic aldehydes (Baktha-

vachalam *et al.*, 1987). The observed *endo* isomers appear to be kinetically favored, since the corresponding *exo*-acetals are presumed to be thermodynamically more stable (Clode, 1979).

Inhibitor (2) was synthesized in six steps as shown in Fig. 3. Conversion of 9-deazainosine to its isopropylidene derivative (9) gave a 79% yield. Benzoylation of (9) produced diester (10) in 75% yield. Subsequent removal of the isopropylidene group in (10) using aqueous trifluoroacetic acid formed (11) in quantitative yield. Reaction of (11) with phosphonoacetaldehyde (6) and concentrated HCl produced acetal (12) in 75% yield, exclusively as the *endo* isomer. The improved yield of acetal in this case may be attributed to the greater stability of the C-nucleoside towards deglycosylation in acid. Compound (12) was debenzoylated using ammonia-saturated methanol to produce (13) in 95% yield. Reaction of (13) with TMSBr led to the target compound (2) in 90% yield.

2.6. Enzyme assay

PNP activity was measured with inosine as the substrate. Hypoxanthine formed in the reaction was oxidized to uric acid by xanthine oxidase. The uric acid concentration was monitored spectrophotometrically at 293 nm to reflect the concentration of the PNP product (Stoeckler *et al.*, 1978). With 0.5 m*M* inosine in 50 m*M* potassium phosphate buffer at pH 7.5 and xanthine oxidase at 0.02 U ml^{-1}, 1 U of PNP activity was defined as the amount of PNP that phosphorolyzes 1 mol inosine per minute at a temperature of 298 K. Specific activity is expressed as units per milligram of protein. The IC_{50} values for the phosphonate inhibitors were determined as described by Montgomery *et al.* (1993).

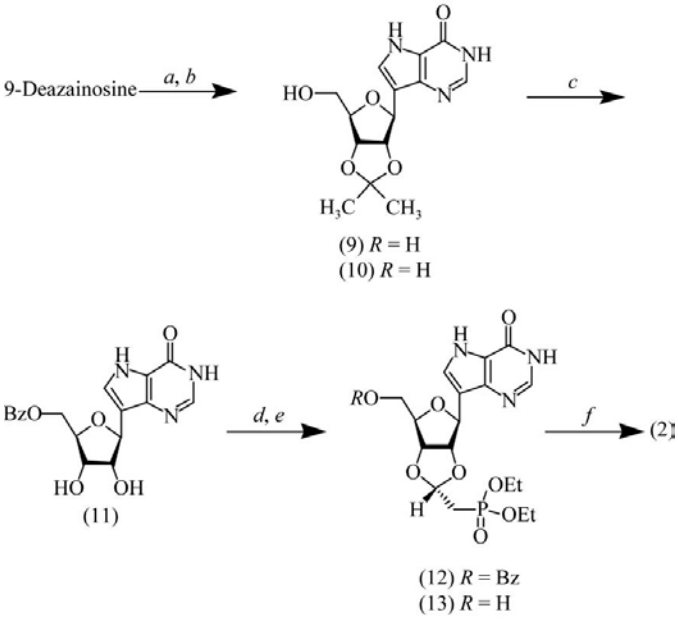

Figure 3
Synthesis of compound (2)

3. Results

3.1. Overall structure

The overall structure of bovine PNP complexed with each of the multisubstrate-analog inhibitors (1, 2 and 3) resembles the previously determined bovine PNP structures (Koellner *et al.*, 1997; Luic *et al.*, 2004; Mao *et al.*, 1998). The refinement statistics for the three complexes are summarized in Table 2. The enzyme is a trimer of identical subunits, with one active site per subunit (Fig. 4*a*). Each monomer has an α/β structure with a central mixed eight-strand β-sheet and a smaller five-

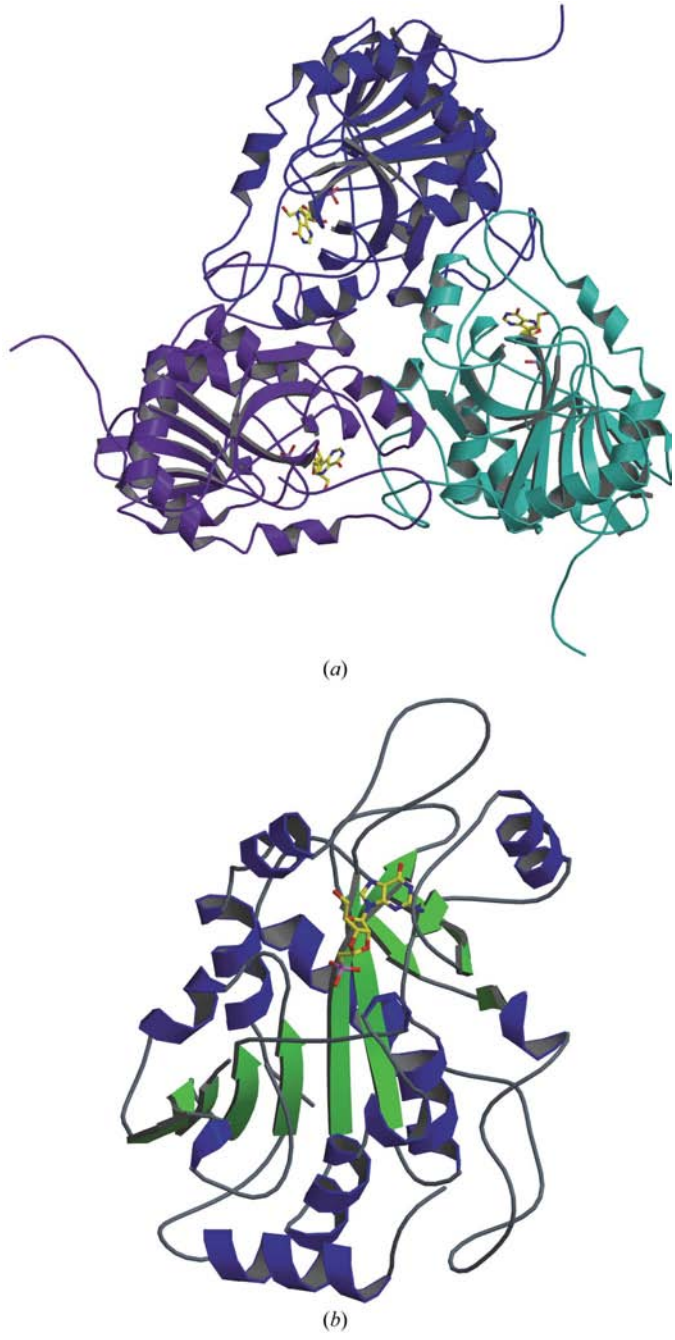

Figure 4
Ribbon diagrams of (*a*) the bovine PNP trimer and (*b*) of the monomer with compound (1) bound.

strand sheet which join to form a distorted β-barrel. Nine α-helices surround this β-barrel structure (Fig. 4*b*).

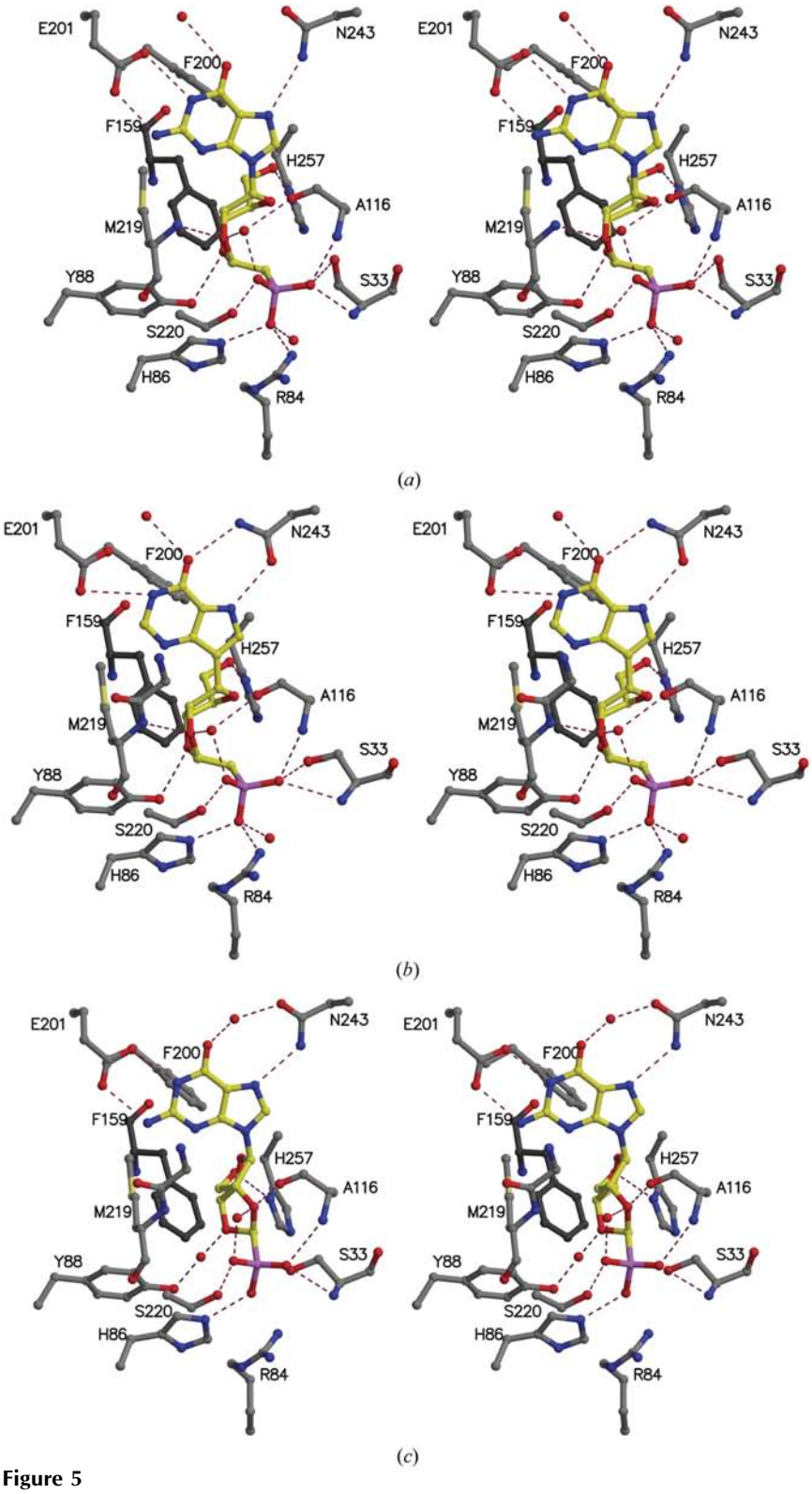

Figure 5
Stereo diagrams of the PNP active site with (*a*) compound (1), (*b*) compound (2) and (*c*) compound (3). The PNP residues are shown in ball-and-stick representation with O atoms in red, C atoms in gray, N atoms in blue and P atoms in purple. The C atoms of the inhibitor are colored yellow. Phe159 from the neighboring subunit is shown in dark gray. Hydrogen bonds are indicated by dashed lines.

The active site of PNP resides in a deep cavity near the subunit–subunit interface. It involves seven polypeptide segments from one subunit and a short segment from an adjacent subunit. Two of the catalytic site loops change conformation upon phosphate binding (residues 30–40 and 58–66), while the conformation of a third loop (residues 244–266) is altered upon nucleoside or base binding. The active site can be divided into three parts: the phosphate-binding site, the ribose-binding site and the base-binding site. The phosphate-binding site is composed of residues Ser33, Arg84, His86 and Ser220. The ribose-binding is amphipathic, consisting of residues Tyr88, Phe159 (from an adjacent subunit), Phe200, His257, Met219 and Glu259. The base-binding site is composed of residues Glu201 and Asn243, which form hydrogen bonds with the purine. The remainder of the purine-binding pocket is largely hydrophobic, consisting of residues Ala116, Ala117, Gly118, Phe200, Val217, Gly218, Met219 and Thr242.

3.2. Structure of the PNP–phosphonate 1 complex

The phosphonate (1) is a multisubstrate-analog inhibitor of PNP. The final model for bovine PNP complexed with inhibitor (1) contains 2111 protein atoms, 131 water molecules and 26 inhibitor atoms. In addition, one magnesium ion, one zinc ion and one Tris molecule were located in the electron density. Both the zinc ion and the Tris molecule are located on special positions (threefold) in the unit cell and were given one third occupancies. Residues 1–2, 60–65 and 283–289 are disordered in the electron density and were not built into the final model. Gln269 and Gln273 showed disordered side chains and were modeled as alanine. The Ramachandran plot reveals that 90.1% of the amino acids adopt favorable main-chain dihedral angles. Thr221 is the only residue falling in the disallowed region. However, the electron density and previously published structures (Mao *et al.*, 1998) strongly support this result. The final model has an R factor of 21.2% and an $R_{\rm free}$ of 25.4%.

The active site of the PNP–phosphonate (1) complex contains one inhibitor molecule and three water molecules. The average B factor for the inhibitor molecule

in the active site is 22.8 Å^2, indicating the inhibitor is bound with high occupancy (see Fig. 6*a*). Fig. 5(*a*) illustrates the interactions between compound (1) and the active-site residues. Compound (1) interacts with residues in all three of the active-site regions: the base-, the ribose- and the phosphate-binding pockets. The guanine moiety of the inhibitor forms three direct hydrogen-bonding interactions with residues in the base-binding pocket. The N7 atom of the inhibitor accepts a hydrogen bond from Asn243 N$^{\delta2}$, while the N2 and N1 atoms donate hydrogen bonds to O$^{\varepsilon1}$ and O$^{\varepsilon2}$ of Glu201, respectively. In addition, the O6 atom is involved in a water-mediated hydrogen bond with Glu201 O$^{\varepsilon2}$. The ribose moiety of the inhibitor is located in the hydrophobic environment created by residues His86, Tyr88, Phe200 and Phe159 (from the neighboring subunit). The sugar moiety of inhibitor (1) is bound in an O4′-*exo* conformation. The O5′ of the ribose moiety forms a hydrogen bond with His257 N$^{\delta1}$. The O2′ atom forms hydrogen-bonding interactions with Met219 N and a water molecule, while the O3′ atom forms a single weak hydrogen bond to Tyr88 OH. The phosphonate moiety forms extensive hydrogen-bonding interactions with the phosphate-binding pocket. The O2 atom of the phosphonate moiety accepts two hydrogen bonds from Ser220 O$^{\gamma}$ and a water molecule. The O3 atom interacts with the main-chain N atoms of Ala116 and Ser33, as well as Ser33 O$^{\gamma}$. Finally, the O4 atom is involved in hydrogen-bonding interactions with His86 N$^{\varepsilon2}$, Arg84 NH1 and a water molecule.

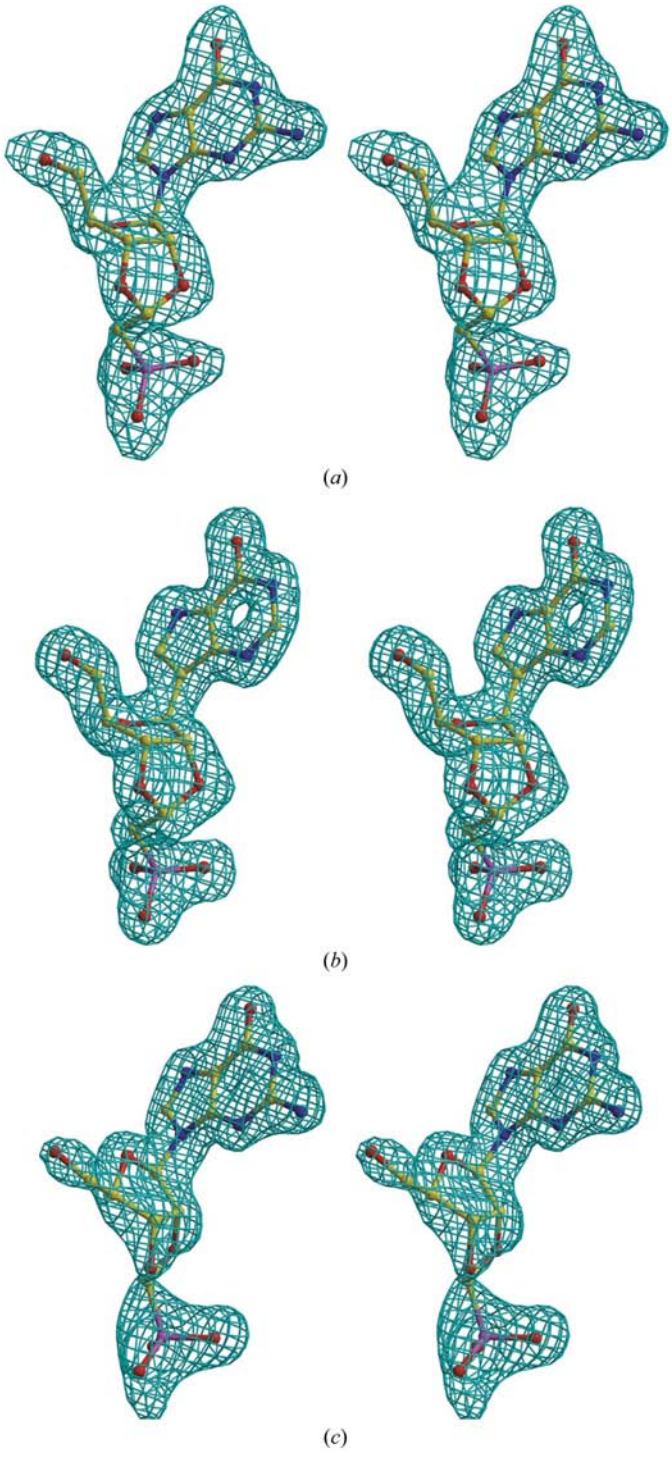

Figure 6
Stereoview of an $F_{obs} - F_{calc}$ electron-density map contoured at 3σ for (*a*) compound (1), (*b*) compound (2) and (*c*) compound (3). For the calculation of the map, the inhibitor molecules were omitted from the model. The atoms are colored according to the scheme described for Fig. 5.

3.3. Structure of the PNP–phosphonate (2) complex

The complex with inhibitor (2) contained 2117 protein atoms, 258 water molecules and 25 inhibitor atoms. Residues 1–2, 60–65 and 283–289 are disordered and were not built into the model. The magnesium and zinc ions as well as the Tris molecule were again observed in the electron density and included in the final model. The Ramachandran plot shows 93.9% of the residues in the most favorable region, with 5.2% in the additionally allowed areas. As with complex (1), Thr221 falls into the disallowed region of the plot, but the conformation is again strongly supported by the electron density.

The overall structure of the the compound (2) complex is very similar to that of compound (1). The active site of the PNP–phosphonate (2) complex also contains one inhibitor molecule and three water molecules. The inhibitor is bound with a high occupancy (see Fig. 6*b*), indicated by the average *B* factor of 26.8 Å^2. Fig. 5(*b*) illustrates the interactions between compound (2) and the active-site residues. The ribose and phosphonate moieties exhibit binding modes nearly identical to that observed for compound (1). The sugar moiety of inhibitor (2) is bound in an O4′-*exo* conformation and the phosphonate moiety makes hydrogen-bonding interactions with Ser33, Arg84, His86, Ala116, Ser220 and two water molecules. The differences in purine binding are a consequence of protonation at N7 of the 9-deazahypoxanthine moiety, resulting in an altered hydrogen-bonding scheme. The N7 atom of the inhibitor donates a hydrogen bond to Asn243 O$^{\delta1}$ and the O6 atom accepts a hydrogen bond from Asn243 N$^{\delta2}$. In addition, the O6 atom of the 9-deazahypoxanthine moiety is involved in a water-mediated hydrogen bond with Glu201 O$^{\varepsilon1}$. The N1 atom donates hydrogen bonds to O$^{\varepsilon}$, as observed in the phosphonate (1) complex.

3.4. Structure of the PNP–phosphonate (3) complex

The final model for the PNP–inhibitor (3) structure contained 2139 protein atoms, 175 water molecules and 25 ligand atoms. Residues 1–2, 60–65, 250–253 and 283–289 are disordered and were not built into the model. The magnesium and zinc ions as well as the Tris molecule observed in the previous two complexes were also included in the final model. The Ramachandran plot shows 92.1% of the residues in the most favorable region, with 6.6% in the additionally allowed areas. A single amino acid, Thr221, falls into the disallowed region of the plot, but the conformation is again strongly supported by the electron density.

Binding of the phosphonate (3) introduces minor main-chain conformational changes in the thermodynamically labile nucleoside-binding active-site loop [the r.m.s.d. between complexes (1) and (3) is 0.3 Å for 270 aligned C^{α} atoms]. The active site of the PNP–phosphonate (3) complex contains one inhibitor molecule and three water molecules. The average *B* factor for the inhibitor is 33.6 $Å^2$, which may indicate a slightly lower occupancy (see Fig. 6*c*). Fig. 5(*c*) illustrates the interactions between compound (3) and the active-site residues. Despite the nonideal linker length between the nucleoside and phosphonate moieties of the inhibitor, compound (3) is still interacts with residues in all three of the active-site binding pockets. However, there are a number of distorted contacts which may result in weaker binding. The phosphonate moiety has shifted 0.5 Å out of the phosphate-binding pocket relative to compound (1) (Fig. 7). The shift results in a loss of hydrogen-bonding contacts with Arg84. The water molecule observed in this region for compounds (1) and (2) is also absent. Thus, the O4 atom of the inhibitor is only involved in one hydrogen-bond interaction with His86 $N^{\varepsilon 2}$. The O2 atom of the phosphonate moiety accepts hydrogen bonds from Ser220 O^{γ} and a water molecule. The O3 atom interacts with the main-chain N atoms of Ala116 and Ser33, but is 3.8 Å away from Ser33 O^{γ}. The conformation of the sugar conformation is distorted from O4′-*exo*, observed for compounds (1) and (2), to C4′-*exo*. The C2′ and C3′ atoms have shifted 1.30 and 0.9 Å, respectively, relative to the binding of compound (1) (Fig. 7). The large movement of the O2′ atom results in the loss of hydrogen-bonding interactions with Met219 N. The environment of the O3′ atom is also altered. The O3′ atom forms a water-mediated rather than a direct hydrogen bond with Tyr88. The O5′ atom exhibits a large movement of 1.6 Å, resulting in a weaker hydrogen bond with His257 $N^{\delta 1}$ (3.0 Å compared with 2.7 Å in compounds 1 and 2). The differences in the hydrogen-bonding scheme of purine binding in compound (3) are a consequence of the movement of the base out of the active site by almost 1 Å. The N7 atom of the inhibitor accepts a hydrogen bond from Asn243 $N^{\delta 2}$, while the N2 and N1 atoms donate hydrogen bonds to $O^{\varepsilon 1}$ and $O^{\varepsilon 2}$ of Glu201, respectively. In addition the O6 atom is involved in a water-mediated hydrogen bond with Asn243 $O^{\varepsilon 1}$.

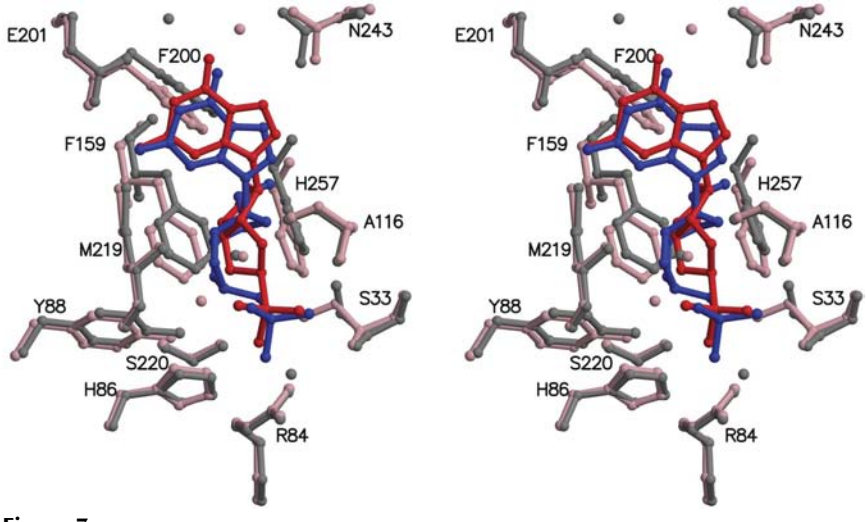

Figure 7
Stereoview of the superposition of compounds (1) and (3). Compound (1) is shown in blue and the surrounding protein residues and water molecules residues in grey. Compound (3) is shown in red and the surrounding protein residues and water molecules in pink.

3.5. Biological assay

The assay results against bovine PNP are listed in Fig. 8. All three compounds are competitive inhibitors of bovine PNP. A comparison of compounds (1) and (3) reveals that the longer chain phosphonic acid derivative shows tenfold better inhibition of the enzyme. Incorporation of the 9-deaza modification of hypoxanthine (compound 2) resulted in an additional order of magnitude improvement in bovine PNP inhibition relative to compound (1).

4. Discussion

4.1. Comparison with the complex of PNP with inosine and sulfate

Inferred hydrogen-bond contacts in the complex with inosine and sulfate are shown in Fig. 9(*a*) (Mao *et al.*, 1998). The complex of PNP with compound (2) superimposed on the complex with inosine and sulfate is shown in Fig. 9(*b*). The base-binding site interactions are nearly identical in the two complexes. One additional hydrogen bond is observed between the N7 atom of compound (2) and Asn243 $O^{\delta 1}$, which results from protonation at N7 of the 9-deazahypoxanthine moiety. Overall, the hydrogen bonds to the base in compound (2) are shorter than observed in the inosine/sulfate complex. The additional ring strain introduced by the cyclic acetal on the ribose moiety in the multisubstrate phosphonate analogs results in some changes in the ribose-binding site. The sugar pucker in the inosine complex is C4′-*endo*; this is distorted to O4′-*exo* in compounds (1) and (2). In addition to the change in sugar pucker, the ribose moiety is also shifted sideways in the pocket by approximately 0.5 Å. As a result of the shift, the hydrogen-bonding interactions with the O2′

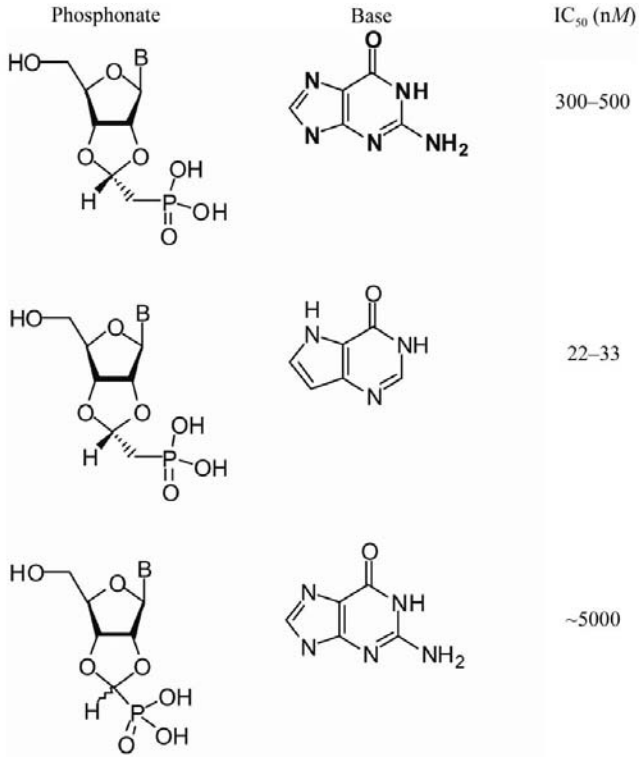

Figure 8
Biological assay.

and O3′ atoms in compounds (1) and (2) are much weaker than those observed for inosine, with the distances increasing by 0.3–0.5 Å. However, the shift does not affect the contacts with the O5′ hydroxyl atom, which is observed in all complexes to make a hydrogen bond with His257 $N^{\delta1}$. The interactions observed in the phosphate-binding pocket are essentially the same between the multisubstrate phosphonate analogs (1) and (2) and the inosine plus sulfate complexes, with the phosphonate group occupying the same location as the sulfate ion (Fig. 9*b*). Thus, the structural comparison confirms that the two-carbon bridge between the ribose ring and the phosphonate group in compounds (1) and (2) is the ideal length for the multisubstrate analog to simultaneously occupy all three active-site regions.

4.2. Comparison with other inhibitors

The design of a potent multisubstrate-analog inhibitor should contain a phosphate-like moiety to take advantage of the extensive hydrogen-bonding interactions within the phosphate-binding pocket of the enzyme. Unfortunately, the susceptibility of nucleoside phosphates to metabolism and their inability to permeate membranes limit their potential as clinically useful inhibitors. The incorporation of a phosphonate moiety in the inhibitor design alleviates the susceptibility to metabolism and may allow their passage across the membrane by esterification of the phosphonate. Moderate inhibitors (K_i^{app} in the micromolar range) have been designed based on acylic nucleoside phosphonates (Bzowska *et al.*, 2000). Improvement of the inhibitory properties of these compounds was achieved by the inclusion of α-fluoro and α,α-difluoro alkanephosphonates (Blackburn & Kent, 1986; Halazy *et al.*, 1991). The structures of PNP in complex with 2,6-diamino-(*S*)-9-[(2-phosphonomethoxy)propyl]-purine [(*S*)-PMPDAP] and 9-(5,5-difluoro-5-phosphonopentyl)guanine (DFPP-G) have recently been published (Bzowska *et al.*, 2004; Luic *et al.*, 2004). Both of these multisubstrate-analog inhibitors consist of a purine base, an acyclic chain and a phosphonate moiety and structural analysis of the binding of these compounds reveals that they occupy the purine-, ribose- and phosphate-binding pockets. While the acyclic chains of (*S*)-PMPDAP and DFPP-G occupy the ribose-binding pocket, they do not form any direct electrostatic interactions with the enzyme. Unlike these acyclic nucleoside phosphonates, compounds (1) and (2) are better able to form direct electrostatic interactions with the ribose-binding pocket as they more closely resemble the true enzyme substrate.

Recently, transition-state analogs have been developed by Schramm and coworkers. Immucillin-H (ImmH) and immucillin-G (ImmG) (Miles *et al.*, 1998) were reported to be the most potent inhibitors for PNP, with K_i values of 23 and 72 p*M*, respectively. The charge of the ribooxocarbenium ion in the transition state (Kline & Schramm, 1995) is mimicked by the iminoribitol moiety. The deazahypoxanthine ring of ImmH is protonated at N7, similar to inosine in the transition state. These electronic features result in ImmH binding to PNP a million times more tightly than to the substrate inosine. Further modification of these compounds has led to the development of 4′-deaza-1′-aza-deoxy-1′-(9-methylene)-immucillin (DADMe-Imm) derivatives. DADMe-ImmG and DADMe-ImmH have been shown to be superior for the inhibition of human PNP with K_d values of 7 and 16 p*M*, respectively (Evans *et al.*, 2003). It is possible that the incorporation of some of the features of the immucillin derivatives into the phosphonate multisubstrate-analog inhibitors reported here would result in further improvements in binding. However, the ring strain introduced into the ribose moiety of compounds (1) and (2) may prevent the iminoribitol phosphonate analogs from binding in the C4′-*endo* conformation as observed in the crystal structure of ImmH bound to bovine PNP (Federov *et al.*, 2001).

5. Conclusions

Inhibitors (1) and (2) were designed based on the X-ray structure of bovine PNP. Compounds (1) and (2) were synthesized in six steps in overall yields of 20 and 50%, respectively. Both compounds showed high activity against bovine PNP, having IC_{50} values of 300 and 30 n*M*, respectively. Compounds (1) and (2) are among the best PNP inhibitors that have been reported. These two compounds have been co-crystallized with PNP and their three-dimensional structures have been determined. The well resolved structures have provided detailed information about binding and confirm the multisubstrate properties designed into the inhibitors.

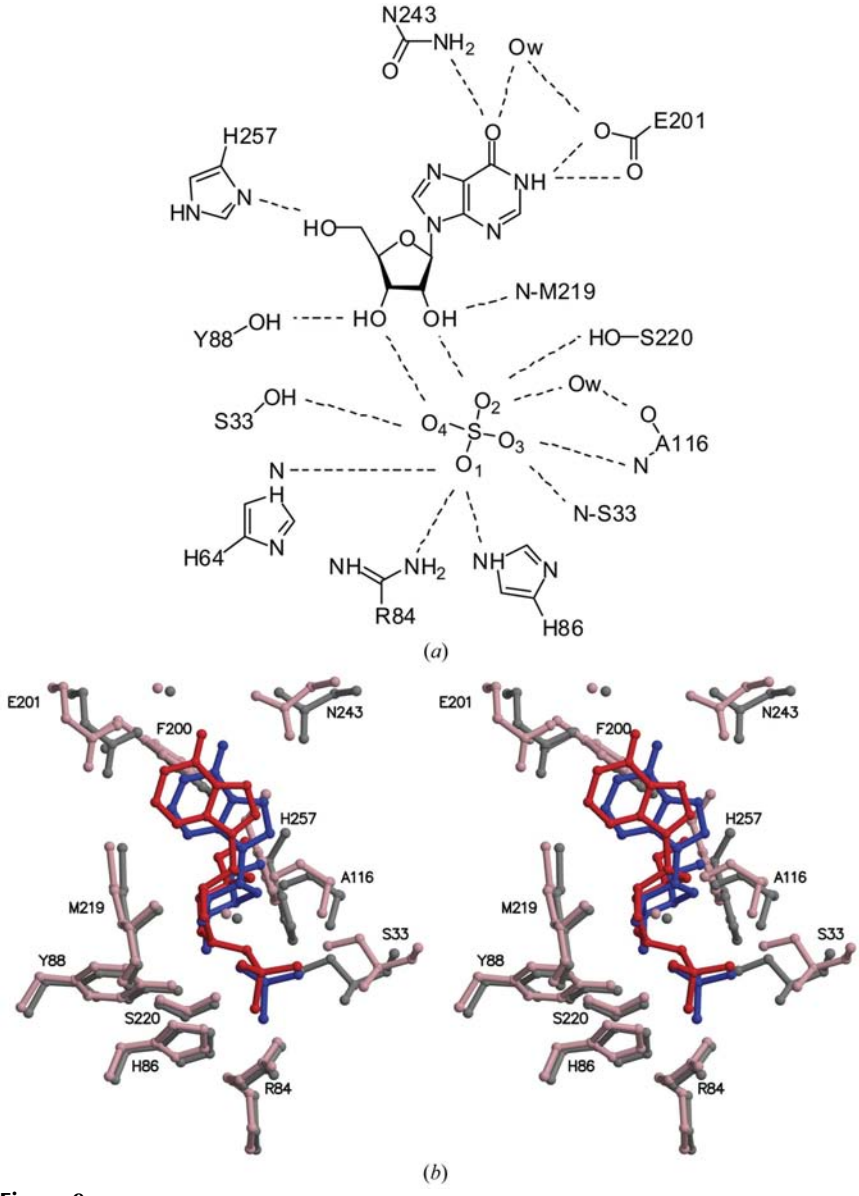

Figure 9
Comparison with the binding of inosine and sulfate. (*a*) Schematic view of the binding of inosine and sulfate in the active site of bovine PNP (PDB code 1a9s). (*b*) Stereoview of the active-site superposition of compound (2) with inosine and sulfate. Compound (2) is shown in red and the surrounding protein in pink. Inosine and sulfate are shown in blue and the surrounding protein residues in gray.

SEE is indebted to the W. M. Keck Foundation and the Lucille P. Markey Charitable Trust. We thank the Cornell High Energy Synchrotron Source for provision of beam time and Leslie Kinsland for assistance in the preparation of this manuscript. Support for this project was also provided by a grant to SEE (2U19CA67763) from the National Institutes of Health.

References

Aalten, D. M. van, Bywater, R., Findlay, J. B., Hendlich, M., Hooft, R. W. & Vriend, G. (1996). *J. Comput. Aided Mol. Des.* **10**, 255–262.
Bakthavachalam, V., Lin, L. G., Cherian, X. M. & Czarnik, A. W. (1987). *Carbohydr. Res.* **170**, 124–135.
Blackburn, G. M. & Kent, D. E. (1986). *J. Chem. Soc. Perkin Trans. 1*, pp. 1913–1917.
Brünger, A. T., Adams, P. D., Clore, G. M., DeLano, W. L., Gros, P., Grosse-Kunstleve, R. W., Jiang, J.-S., Kuszewski, J., Nilges, M., Pannu, N. S., Read, R. J., Rice, L. M., Simonson, T. & Warren, G. L. (1998). *Acta Cryst.* D**54**, 905–921.
Bzowska, A., Koellner, G., Wielgus-Kutrowska, B., Stroh, A., Raszewski, G., Holy, A., Steiner, T. & Frank, J. (2004). *J. Mol. Biol.* **342**, 1015–1032.
Bzowska, A., Kulikowska, E. & Shugar, D. (2000). *Pharmacol. Ther.* **88**, 349–425.
Bzowska, A., Luic, M., Schroder, W., Shugar, D., Saenger, W. & Koellner, G. (1995). *FEBS Lett.* **367**, 214–218.
Cacciapuoti, G., Porcelli, M., Bertoldo, C., De Rosa, M. & Zappia, V. (1994). *J. Biol. Chem.* **269**, 24762–24769.
Chladek, S. & Smrt, J. (1964). *Collect. Czech. Chem. Commum.* **29**, 214–233.
Clode, D. M. (1979). *Chem. Rev.* **79**, 491–513.
Cohen, A., Gudas, L. J., Ammann, A. J., Staal, G. E. & Martin, D. W. Jr (1978). *J. Clin. Invest.* **61**, 1405–1409.
Ealick, S. E., Babu, Y. S., Bugg, C. E., Erion, M. D., Guida, W. C., Montgomery, J. A. & Secrist, J. A. III (1991). *Proc. Nat. Acad. Sci. USA*, **88**, 11540–11544.
Ealick, S. E., Rule, S. A., Carter, D. C., Greenhough, T. J., Babu, Y. S., Cook, W. J., Habash, J., Helliwell, J. R., Stoeckler, J. D. & Bugg, C. E. (1990). *J. Biol. Chem.* **265**, 1812–1820.
Endova, M., Masojidkova, M., Budesinsky, M. & Rosenberg, I. (1996). *Tetrahedron Lett.* **37**, 3497–3500.
Evans, G. B., Furneaux, R. H., Lewandowicz, A., Schramm, V. L. & Tyler, P. C. (2003). *J. Med. Chem.* **46**, 5271–5276.
Federov, A., Shi, W., Kicska, G., Tyler, P. C., Furneaux, R. H., Hanson, J. C., Gainsford, G. J., Larese, J. Z., Schramm, V. L. & Almo, S. C. (2001). *Biochemistry*, **40**, 853–860.
Giblett, E. R., Ammann, A. J., Wara, D. W., Sandman, R. & Diamon, L. K. (1975). *Lancet*, **1**, 1010–1013.
Halazy, S., Ehrhard, A. & Danzin, C. (1991). *J. Am. Chem. Soc.* **113**, 315–317.
Hori, N., Watanabe, M., Yamazaki, Y. & Mikami, Y. (1989). *Agric. Biol. Chem.* **53**, 2205–2210.
Jensen, K. F. (1978). *Biochim. Biophys. Acta*, **525**, 346–356.
Jensen, K. F. & Nygaard, P. (1975). *Eur. J. Biochem.* **51**, 253–265.
Jones, T. A., Zou, J.-Y., Cowan, S. W. & Kjeldgaard, M. (1991). *Acta Cryst.* A**47**, 110–119.
Kline, P. C. & Schramm, V. L. (1995). *Biochemistry*, **34**, 1153–1162.
Koellner, G., Luic, M., Shugar, D., Saenger, W. & Bzowska, A. (1997). *J. Mol. Biol.* **265**, 202–216.
Laskowski, R. A., MacArthur, M. W., Moss, D. S. & Thornton, J. M. (1993). *J. Appl. Cryst.* **26**, 283–291.
Luić, M., Koellner, G., Yokomatsu, T., Shibuya, S. & Bzowska, A. (2004). *Acta Cryst.* D**60**, 1417–1424.
Mao, C., Cook, W. J., Zhou, M., Federov, A. A., Almo, S. C. & Ealick, S. E. (1998). *Biochemistry*, **37**, 7135–7146.
Miles, R. W., Tyler, P. C., Furneaux, R. H., Bagdassarian, C. K. & Schram, V. L. (1998). *Biochemistry*, **37**, 8615–8621.

Montgomery, J. A., Niwas, S., Rose, J. D., Secrist, J. A. III, Babu, Y. S., Bugg, C. E., Erion, M. D., Guida, W. C. & Ealick, S. E. (1993). *J. Med. Chem.* **36**, 55–69.
Otwinowski, Z. & Minor, W. (1997). *Methods Enzymol.* **276**, 307–326.
Read, R. J. (1986). *Acta Cryst.* A**42**, 140–149.
Senesi, S., Falcone, G., Mura, U., Sgarrella, F. & Ipata, P. L. (1976). *FEBS Lett.* **64**, 353–357.
Stoeckler, J. D. (1984). *Development in Cancer Chemotherapy*, edited by R. E. Glazer, pp. 35–60. Boca Raton, FL, USA: CRC Press.
Stoeckler, J. D., Agarwal, R. P., Agarwal, K. C. & Parks, R. E. Jr (1978). *Methods Enzymol.* **51**, 530–538.
Tuttle, J. V. & Krenitsky, T. A. (1984). *J. Biol. Chem.* **259**, 4065–4069.
Yanai, S., Halmann, M. & Vofsi, D. (1980). *Carbohydr. Res.* **83**, 243–248.